Dalton Transactions

PAPER

View Article Online
View Journal | View Issue

Cite this: *Dalton Trans.*, 2015, **44**, 13853

Aza-macrocyclic complexes of the Group 1 cations – synthesis, structures and density functional theory study†

John Dyke,[a] William Levason,[a] Mark E. Light,[a] David Pugh,[a] Gillian Reid,*[a] Hanusha Bhakhoa,[b] Ponnadurai Ramasami[b] and Lydia Rhyman[b]

The Group 1 complexes, $[M(Me_6[18]aneN_6)][BAr^F]$ (M = Li–Cs; $Me_6[18]aneN_6$ = 1,4,7,10,13,16-hexamethyl-1,4,7,10,13,16-hexaazacyclooctadecane; BAr^F = tetrakis{3,5-bis(trifluoromethyl)-phenyl}borate), are obtained in high yield by reaction of the macrocycle with $M[BAr^F]$ in anhydrous CH_2Cl_2 solution, and characterised spectroscopically (^1H, $^{13}C\{^1H\}$, ^7Li, ^{23}Na, and ^{133}Cs NMR), by microanalysis and, for M = Li, K, and Rb, by single crystal X-ray analysis. The structures show N_6-coordination to the metal ion; the small ionic radius for Li^+ leads to a puckered conformation. In contrast, the K^+ ion fits well into the N_6 plane, with the $[BAr^F]^-$ anions above and below, leading to two K^+ species in the asymmetric unit (a hexagonal planar $[K(Me_6[18]aneN_6)]^+$ cation and a '$[K(Me_6[18]aneN_6)(\kappa^1\text{-}BAr^F)_2]^-$ anion', with long axial K···F interactions). The Rb^+ ion sits above the N_6 plane, with two long axial Rb···F interactions in one cation and two long, mutually *cis* Rb···F interactions in the other. The unusual sandwich cations, $[M(Me_3tacn)_2]^+$ (M = Na, K; distorted octahedral, N_6 donor set) and half-sandwich cations $[Li(Me_3tacn)(thf)]^+$ (distorted tetrahedron, N_3O donor set), $[Li(Me_4cyclen)(OH_2)]^+$, and $[Na(Me_4cyclen)(thf)]^+$ (both distorted square pyramids with N_4O donor sets) were also prepared (Me_3tacn = 1,4,7-trimethyl-1,4,7-triazacyclononane, $Me_4cyclen$ = 1,4,7,10-tetramethyl-1,4,7,10-tetraazacyclododecane). Density functional theory (DFT) calculations, using the BP86 and B3LYP functionals, show that the accessibility of the $[M(Me_3tacn)_2]^+$ sandwich cations depends strongly on the M^+ ionic radius, such that it is sufficiently large to avoid steric clashing between the Me groups of the two rings, and small enough to avoid very acute N–M–N chelate angles. The calculations also show that coordination to the Group 1 cation involves significant donation of electron density from the p-orbitals on the N atoms of the macrocycle, rather than purely electrostatic interactions.

Received 18th May 2015,
Accepted 15th June 2015

DOI: 10.1039/c5dt01865j

www.rsc.org/dalton

Introduction

The coordination chemistry of Group 1 cations with *neutral* ligands is dominated by oxygen-donor ligands such as alcohols, ethers, and water, including the ubiquitous crown ethers and cryptands which are frequently used as ligands towards Group 1 cations.[1,2] The corresponding chemistry with the less electronegative neutral polyaza macrocycles has been much less studied. We recently reported the preparation of several unusual complexes based upon coordination of Na^+ to Me_3tacn (1,4,7-trimethyl-1,4,7-triazacyclononane) and Me_4cyclam (1,4,8,11-tetramethyl-1,4,8,11-tetraazacyclotetradecane), including structural characterisation of the sandwich cation salt, $[Na(Me_3tacn)_2][BAr^F]$ (BAr^F = tetrakis{3,5-bis(trifluoromethyl)phenyl}borate) and $[Na(Me_4cyclam)(thf)][BAr^F]$, containing tetradentate coordination of the macrocycle.[3] The Me_3tacn complexes were initially isolated serendipitously from reactions of $Na[BAr^F]$ with $SiCl_4$ in the presence of the N-donor macrocycles, towards preparation of potential precursors for the supercritical fluid electrodeposition (SCFED) of semiconductor materials.[4] The Na^+ preferentially coordinated to the N-donor macrocycle, and we attributed this unusual behaviour to the low lattice energy of $Na[BAr^F]$, coupled with the high solubility of the $[BAr^F]^-$ salts in non-competitive, very weakly coordinating solvents, such as CH_2Cl_2 and toluene.

Neutral diamines (*e.g.* *N*,*N*,*N*′,*N*′-tetramethylethylenediamine) are often used as complexation agents to increase the reactivity of alkyl lithiums[5] and to increase the solubility of

[a]*Chemistry, University of Southampton, Highfield, Southampton, SO17 1BJ, UK. E-mail: G.Reid@soton.ac.uk*
[b]*Computational Chemistry Group, Department of Chemistry, Faculty of Science, University of Mauritius, Réduit 80837, Mauritius*

†Electronic supplementary information (ESI) available: X-ray crystallographic parameters and cif files for the complexes reported (Table S1), crystallographic data in CIF format, together with full DFT computational details using both the BP86 and B3LYP functionals (Tables S2–S30, Fig. S1–S5). CCDC 1051099–1051104. For ESI and crystallographic data in CIF or other electronic format see DOI: 10.1039/c5dt01865j

heavier Group 1 alkyls.[6] Whilst a small number of pendant arm functionalised N-donor macrocycles are known to form complexes with alkali metal cations,[7] complexes of *neutral* N-donor macrocycles with these cations have been very little studied. Earlier work has shown that *N*-methylated aza macrocycles are more stable towards electrides compared to the analogous crown ethers.[8] Other than the two Na^+-aza macrocyclic complexes that we reported,[3] four examples involving Me_3tacn coordinated to lithium are known: two lithium-based electrides, a BzLi complex with Me_3tacn and a lithium enolate stabilised by Me_3tacn.[9] Two sodium complexes with Me_3tacn and Me_3cyclen (1,4,7-trimethyl-1,4,7,10-tetraazacyclododecane) were structurally characterised.[10] No examples of neutral tri- and tetra-aza macrocycles are known for K^+, Rb^+, or Cs^+ and there are very few examples with the *N*-methylated aza analogue of 18-crown-6, Me_6[18]aneN_6 (1,4,7,10,13,16-hexamethyl-1,4,7,10,13,16-hexaazacyclooctadecane).[8,11] The crystal structures of two electrides, $[K(Me_6[18]aneN_6)]^+Na^-$ and $[Cs(Me_6[18]aneN_6)]^+Na^-$, were determined by Dye and co-workers,[11a] who also reported NMR spectroscopic evidence for $[Rb(Me_6[18]aneN_6)]^+Na^-$, $[Cs(Me_6[18]aneN_6)]^+$, $[Cs(Me_6[18]aneN_6)_2]^+$, and two $[Cs(Me_6[18]aneN_6)(crown)]^+$ complexes.[11b,c,8]

We report here the first systematic study of the synthesis, spectroscopic, and structural characterisation of Group 1 cation (Li^+ to Cs^+) complexes involving tri-, tetra- and hexa-aza macrocycles. Density functional theory (DFT) with the BP86 and B3LYP functionals has been used to investigate the electronic structure and bonding present in the resulting cations.

Experimental

All preparations were carried out under a dry dinitrogen atmosphere using standard Schlenk and glove box techniques. $[Li(thf)_4][BAr^F]$ and $Na[BAr^F]$·2thf were synthesised using a slight modification of the literature procedure.[12] The lithium salt was isolated as $[Li(OH_2)_4][BAr^F]$, which can be converted to the thf adduct by stirring in thf for 16 h over 4 Å molecular sieves. Filtration and removal of solvents affords the thf adduct. Crude $Na[BAr^F]$ was recrystallised from thf/*n*-hexane, resulting in the isolation of $Na[BAr^F]$·2thf. $K[BAr^F]$, $Rb[BAr^F]$, and $Cs[BAr^F]$ were synthesised *via* cation exchange of $Na[BAr^F]$·2thf in water at 95 °C with excess (5 mol. equiv.) KNO_3, $RbNO_3$, or $CsNO_3$, respectively.[13] Me_3tacn was synthesised by a literature procedure.[14] Me_4cyclen was obtained by methylation of cyclen (Sigma) using formic acid/formaldehyde.[15] Me_6[18]aneN_6 (Sigma) was used as received. CH_2Cl_2 was dried by distillation from CaH_2, toluene distilled from Na, and *n*-hexane distilled from Na/K alloy. ^1H and $^{13}C\{^1H\}$ NMR spectra were recorded in CD_2Cl_2 solution at 298 K using a Bruker AV II-400 spectrometer and are referenced to the residual CH_2Cl_2 resonance. ^7Li, ^{23}Na, and ^{133}Cs NMR spectra were obtained on a Bruker AV II-400 spectrometer at 298 K (unless otherwise stated) and referenced to a 0.1 mol dm^{-3} solution of LiCl, NaCl, or $CsNO_3$ in D_2O, respectively. Microanalyses were undertaken at London Metropolitan University.

X-ray crystallography

Crystals were obtained as described below. Details of the crystallographic data collection and refinement are in Table S1.† Diffractometer: *Rigaku AFC12* goniometer equipped with an enhanced sensitivity (HG) *Saturn724+* detector mounted at the window of an *FR-E+ SuperBright* molybdenum rotating anode generator (λ_1 = 0.71073 Å) with VHF *Varimax* optics (70 μm focus). Cell determination and data collection: CrystalClear-SM Expert 3.1 b27, data reduction, cell refinement, and absorption correction: CrystalClear-SM Expert 2.1 b29.[16] Structure solution and refinement were carried out using WinGX and software packages within.[17] Disorder in the CF_3 groups of the $[BAr^F]^-$ anions was present in all of the structures, which is often observed in compounds containing $[BAr^F]^-$,[18] and this was satisfactorily modelled using DFIX, DELU, and SIMU restraints. Positional disorder was also present in the $-CH_2CH_2-$ linkers of the macrocycle in $[Na(Me_4cyclen)(thf)][BAr^F]$ and was modelled similarly. Two locations for the water molecule in $[Li(Me_4cyclen)(H_2O)][BAr^F]$ were observed, with the combined electron density consistent with one fully-occupied water molecule. Attempts to model this as other moieties (*e.g.* methoxide) were unsuccessful. H-atoms were placed in geometrically-assigned positions with C–H distances of 0.95 Å (CH), 0.98 Å (CH_2), or 0.99 Å (CH_3) and refined using a riding model with $U_{iso}(H) = 1.2U_{eq.}(C)$ (CH, CH_2) or $1.5U_{eq.}(C)$ (CH_3). enCIFer was used to prepare material for publication.[19] CCDC reference numbers 1051099–1051104 contain crystallographic data in CIF format.

Preparations

$[Li(Me_6[18]aneN_6)][BAr^F]$. $[Li(thf)_4][BAr^F]$ (100 mg, 0.09 mmol) was suspended in CH_2Cl_2 (5 mL) and a solution of Me_6[18]aneN_6 (31 mg, 0.09 mmol) in CH_2Cl_2 (2 mL) was added. The reaction was stirred for 4 h then the product was precipitated by the addition of *n*-hexane (20 mL). Crystals were obtained by layering a concentrated CH_2Cl_2 solution of the product with *n*-hexane. White solid. Yield: 97 mg, 89%. Required for $C_{50}H_{54}BF_{24}LiN_6$: C, 49.51; H, 4.49; N, 6.93. Found: C, 49.52; H, 4.58; N, 6.94%. ^1H NMR (298 K, CD_2Cl_2): δ = 7.73 ([8H], s, BAr^F H2/6), 7.57 ([4H], s, BAr^F H4), 2.46 ([24H], br s, NCH_2), 2.29 ([18H], s, NMe). $^{13}C\{^1H\}$ NMR (298 K, CD_2Cl_2): δ = 162.37 (C, q, J_{C-B} = 49.9 Hz, BAr^F C1), 135.40 (CH, BAr^F C2/6), 129.49 (C, qq, $^2J_{C-F}$ = 31.5, 2.9 Hz, BAr^F C3/5), 125.20 (C, q, J_{C-F} = 272 Hz, CF_3), 118.06 (CH, septet, $^3J_{C-F}$ = 4.0 Hz, BAr^F C4), 56.62 (NCH_2), 45.24 (NMe). ^7Li (298 K, CD_2Cl_2): δ = −0.30.

$[Na(Me_6[18]aneN_6)][BAr^F]$. Prepared similarly using $Na[BAr^F]$·2thf (100 mg, 0.10 mmol) and Me_6[18]aneN_6 (34 mg, 0.10 mmol). Colourless crystals were obtained by layering a concentrated CH_2Cl_2 solution of the product with *n*-hexane. Yield: 59 mg, 44%. Required for $C_{50}H_{54}BF_{24}N_6Na$: C, 48.87; H, 4.43; N, 6.84. Found: C, 48.96; H, 4.35; N, 6.78. ^1H NMR (298 K, CD_2Cl_2): δ = 7.73 ([8H], s, BAr^F H2/6), 7.57 ([4H], s, BAr^F H4), 2.54 ([12H], v br s, NCH_2), 2.26 ([30H], br s, NMe + NCH_2). $^{13}C\{^1H\}$ NMR (298 K, CD_2Cl_2): δ = 162.85 (C, q, J_{C-B} = 49.9 Hz,

BAr^F C1), 135.39 (CH, BAr^F C2/6), 129.38 (C, qq, $^2J_{C-F}$ = 31.5, 2.9 Hz, BAr^F C3/5), 125.20 (C, q, J_{C-F} = 272 Hz, CF_3), 118.05 (CH, septet, $^3J_{C-F}$ = 4.0 Hz, BAr^F C4), 54.16 (NCH_2), 44.22 (NMe). ^{23}Na (298 K, CD_2Cl_2): δ = +3.1.

[K(Me$_6$[18]aneN$_6$)][BAr^F]. Prepared similarly using K[BAr^F] (50 mg, 0.05 mmol) and Me_6[18]aneN$_6$ (17 mg, 0.05 mmol). White crystalline solid. Yield: 51 mg, 76%. Required for $C_{50}H_{54}BF_{24}KN_6$: C, 48.24; H, 4.37; N, 6.75. Found: C, 48.33; H, 4.43; N, 6.68%. ^{1}H NMR (298 K, CD_2Cl_2): δ = 7.72 ([8H], s, BAr^F H2/6), 7.57 ([4H], s, BAr^F H4), 2.68–2.87, 2.15–2.24 (both [9H], v br s, NCH_2), 2.07 ([18H], br s, NMe). ^{13}C{^{1}H} NMR (298 K, CD_2Cl_2): δ = 162.36 (C, q, J_{C-B} = 49.9 Hz, BAr^F C1), 135.39 (CH, BAr^F C2/6), 129.46 (C, qq, $^2J_{C-F}$ = 31.5, 2.9 Hz, BAr^F C3/5), 125.20 (C, q, J_{C-F} = 272 Hz, CF_3), 118.07 (CH, septet, $^3J_{C-F}$ = 4.0 Hz, BAr^F C4), 56.17 (NCH_2), 38.16 (NMe).

[Rb(Me$_6$[18]aneN$_6$)][BAr^F]. Prepared similarly using Rb[BAr^F] (104 mg, 0.10 mmol) and Me_6[18]aneN$_6$ (34 mg, 0.10 mmol). White crystalline solid. Yield: 77 mg, 56%. Required for $C_{50}H_{54}BF_{24}N_6Rb$: C, 46.50; H, 4.21; N, 6.51. Found: C, 46.60; H, 4.24; N, 6.45%. ^{1}H NMR (298 K, CD_2Cl_2): δ = 7.73 ([8H], s, BAr^F H2/6), 7.57 ([4H], s, BAr^F H4), 2.59–2.99, 2.10–2.56 (both [12H], v br m, NCH_2), 2.05 ([18H], s, NMe). ^{13}C{^{1}H} NMR (298 K, CD_2Cl_2): δ = 162.36 (C, q, J_{C-B} = 49.9 Hz, BAr^F C1), 135.41 (CH, BAr^F C2/6), 129.47 (C, qq, $^2J_{C-F}$ = 31.5, 2.9 Hz, BAr^F C3/5), 125.20 (C, q, J_{C-F} = 272 Hz, CF_3), 118.08 (CH, septet, $^3J_{C-F}$ = 4.0 Hz, BAr^F C4), 57.0 (broad, NCH_2), 38.4 (broad, NMe).

[Cs(Me$_6$[18]aneN$_6$)][BAr^F]. Prepared similarly using Cs[BAr^F] (110 mg, 0.10 mmol) and Me_6[18]aneN$_6$ (34 mg, 0.10 mmol). White crystalline solid. Yield: 81 mg, 56%. Required for $C_{50}H_{54}BCsF_{24}N_6$: C, 44.86; H, 4.06; N, 6.28. Found: C, 44.96; H, 3.99; N, 6.23. ^{1}H NMR (298 K, CD_2Cl_2): δ = 7.73 ([8H], s, BAr^F H2/6), 7.57 ([4H], s, BAr^F H4), 2.40 ([18H], v br s, NCH_2), 2.03 ([18H], s, NMe); (183 K): 7.75 ([8H], s, BAr^F H2/6), 7.56 ([4H], s, BAr^F H4), 2.80–3.00 ([2H], m, NCH_2), 2.52–2.76 ([10H], m, NCH_2), 2.00 ([9H], s, NMe), 1.78–1.96 ([17H], m, NCH_2 and NMe), 1.56–1.71 ([4H], m, NCH_2). ^{13}C{^{1}H} NMR (298 K, CD_2Cl_2): δ = 162.36 (C, q, J_{C-B} = 49.9 Hz, BAr^F C1), 135.42 (CH, BAr^F C2/6), 129.48 (C, qq, $^2J_{C-F}$ = 31.5, 2.9 Hz, BAr^F C3/5), 125.21 (C, q, J_{C-F} = 272 Hz, CF_3), 118.08 (CH, septet, $^3J_{C-F}$ = 4.0 Hz, BAr^F C4), 56.79 (broad, NCH_2), 40.3 (broad, NMe). ^{133}Cs NMR (298 K, CD_2Cl_2): δ = 54.0 (s); (183 K): 73.3, 58.7 (both s).

[Li(Me$_3$tacn)(thf)][BAr^F]. [Li(thf)$_4$][BAr^F] (100 mg, 0.09 mmol) was dissolved in toluene (5 mL) and a solution of Me_3tacn (30 mg, 0.17 mmol) in CH_2Cl_2 (2 mL) was added. The reaction was stirred for 4 h then *n*-hexane (20 mL) was added to precipitate a white solid which was isolated by decanting the supernatant and drying *in vacuo*. Yield: 79 mg, 81%. Required for $C_{45}H_{41}BF_{24}LiN_3O$: C, 48.53; H, 3.71; N, 3.77. Found: C, 48.62; H, 3.80; N, 3.82%. ^{1}H NMR (298 K, CD_2Cl_2): δ = 7.73 ([8H], s, BAr^F H2/6), 7.57 ([4H], s, BAr^F H4), 3.73–3.76 ([4H], m, OCH_2), 2.59–2.67, 2.44–2.52 (each [6H], m, NCH_2), 2.41 ([9H], s, NMe), 1.87–1.91 ([4H], m, $OCH_2C\underline{H}_2$). ^{13}C{^{1}H} NMR (298 K, CD_2Cl_2): δ = 162.35 (C, q, J_{C-B} = 49.9 Hz, BAr^F C1), 135.39 (CH, BAr^F C2/6), 129.48 (C, qq, $^2J_{C-F}$ = 31.5, 2.9 Hz, BAr^F C3/5), 125.20 (C, q, J_{C-F} = 272 Hz, CF_3), 118.08 (CH, septet, $^3J_{C-F}$ = 4.0 Hz, BAr^F C4), 68.95 (OCH_2), 54.99 (NCH_2), 45.99 (NMe), 26.02 ($OCH_2\underline{C}H_2$). ^{7}Li NMR (298 K, CD_2Cl_2): δ = +1.47.

[K(Me$_3$tacn)$_2$][BAr^F]. K[BAr^F] (250 mg, 0.24 mmol) was suspended in CH_2Cl_2 (5 mL) and a solution of Me_3tacn (60 mg, 0.48 mmol) in CH_2Cl_2 (2 mL) was added. The reaction was stirred for 4 h then the product was precipitated by the addition of *n*-hexane (30 mL). Crystals were obtained by layering a concentrated CH_2Cl_2 solution of the product with *n*-hexane. White solid. Yield: 239 mg, 81%. Required for $C_{50}H_{54}BF_{24}KN_6$: C, 48.24; H, 4.37; N, 6.75. Found: C, 48.12; H, 4.23; N, 6.66%. ^{1}H NMR (298 K, CD_2Cl_2): δ = 7.74 ([8H], s, BAr^F H2/6), 7.58 ([4H], s, BAr^F H4), 2.48 ([24H], s, NCH_2), 2.37 ([18H], s, NMe). ^{13}C{^{1}H} NMR (298 K, CD_2Cl_2): δ = 162.38 (C, q, J_{C-B} = 49.9 Hz, BAr^F C1), 135.44 (CH, BAr^F C2/6), 129.50 (C, qq, $^2J_{C-F}$ = 31.6, 2.9 Hz, BAr^F C3/5), 125.23 (C, q, J_{C-F} = 272 Hz, CF_3), 118.09 (CH, septet, $^3J_{C-F}$ = 4.0 Hz, BAr^F C4), 54.36 (NCH_2), 46.22 (NMe).

[Li(Me$_4$cyclen)(OH$_2$)][BAr^F]. [Li(OH$_2$)$_4$][BAr^F] (150 mg, 0.16 mmol) was dissolved in CH_2Cl_2 (5 mL) and a solution of Me_4cyclen (36 mg, 0.16 mmol) in CH_2Cl_2 (2 mL) was added. The reaction was stirred for 4 h then all volatiles were removed. Crystals were obtained by layering a concentrated CH_2Cl_2 solution of the product with *n*-hexane. White solid. Yield: 151 mg, 81%. Required for $C_{44}H_{42}BF_{24}LiN_4O$: C, 46.57; H, 3.91; N, 4.94. Found: C, 46.67; H, 3.93; N, 4.82%. ^{1}H NMR (298 K, CD_2Cl_2): δ = 7.74 ([8H], s, BAr^F H2/6), 7.58 ([4H], s, BAr^F H4), 2.52–2.59, 2.28–2.37 (each [8H], m, NCH_2), 2.27 ([12H], s, NMe). ^{13}C{^{1}H} NMR (298 K, CD_2Cl_2): δ = 162.40 (C, q, J_{C-B} = 49.9 Hz, BAr^F C1), 135.44 (CH, BAr^F C2/6), 129.54 (C, qq, $^2J_{C-F}$ = 31.5, 2.9 Hz, BAr^F C3/5), 125.25 (C, q, J_{C-F} = 272 Hz, CF_3), 118.13 (CH, septet, $^3J_{C-F}$ = 4.0 Hz, BAr^F C4), 53.98 (NCH_2), 43.46 (NMe). ^{7}Li NMR (298 K, CD_2Cl_2): δ = +0.41.

[Na(Me$_4$cyclen)(thf)][BAr^F]. Na[BAr^F]·2thf (250 mg, 0.24 mmol) was suspended in CH_2Cl_2 (5 mL) and a solution of Me_4cyclen (55 mg, 0.24 mmol) in CH_2Cl_2 (2 mL) was added. The reaction was stirred for 4 h then the product was precipitated by the addition of *n*-hexane (30 mL). Crystals were obtained by layering a concentrated CH_2Cl_2 solution of the product with *n*-hexane. White solid. Yield: 219 mg, 77%. Required for $C_{48}H_{48}BF_{24}N_4NaO$: C, 48.58; H, 4.08; N, 4.72. Found: C, 48.36; H, 3.98; N, 4.82%. ^{1}H NMR (298 K, CD_2Cl_2): δ = 7.73 ([8H], s, BAr^F H2/6), 7.57 ([4H], s, BAr^F H4), 3.66–3.72 ([4H] m, OCH_2), 2.68 ([6H], s, NCH_2), 2.53–2.59 ([4H], m, NCH_2), 2.46 ([6H], s, NCH_2), 2.27 ([12H], s, NMe), 1.80–1.86 ([4H], m, $OCH_2C\underline{H}_2$). ^{13}C{^{1}H} NMR (298 K, CD_2Cl_2): δ = 162.36 (C, q, J_{C-B} = 49.9 Hz, BAr^F C1), 135.41 (CH, BAr^F C2/6), 129.48 (C, qq, $^2J_{C-F}$ = 31.5, 2.9 Hz, BAr^F C3/5), 125.21 (C, q, J_{C-F} = 272 Hz, CF_3), 118.09 (CH, septet, $^3J_{C-F}$ = 4.0 Hz, BAr^F C4), 68.52 (OCH_2), 53.71 (NCH_2), 43.47 (NMe), 26.14 ($OCH_2C\underline{H}_2$). ^{23}Na NMR (298 K, CD_2Cl_2): δ = +12.7.

[Me$_4$cyclenH][BAr^F]. K[BAr^F] (250 mg, 0.24 mmol) was suspended in CH_2Cl_2 (5 mL) and a solution of Me_4cyclen (70 mg, 0.60 mmol) in CH_2Cl_2 (2 mL) was added. The reaction was stirred for 4 h then concentrated to ~5 mL, *n*-hexane was layered on top and some colourless crystals were obtained. Required for $C_{44}H_{41}BF_{24}N_4$: C, 48.36; H, 3.78; N, 5.13. Found:

C, 48.21; H, 3.58; N, 5.25%. ^{1}H NMR (298 K, CD_2Cl_2): δ = 9.55 ([1H], br s, NH), 7.73 ([8H], s, BAr^F H2/6), 7.57 ([4H], s, BAr^F H4), 2.69 ([16H], s, NCH_2), 2.46 ([12H], s, NMe). $^{13}C\{^1H\}$ NMR (298 K, CD_2Cl_2): δ = 162.35 (C, q, J_{C-B} = 49.9 Hz, BAr^F C1), 135.39 (CH, BAr^F C2/6), 129.48 (C, qq, $^2J_{C-F}$ = 31.6, 2.9 Hz, BAr^F C3/5), 125.20 (C, q, J_{C-F} = 272 Hz, CF_3), 118.11 (CH, septet, $^3J_{C-F}$ = 4.0 Hz, BAr^F C4), 54.03 (NCH_2), 43.44 (NMe). The same product was also obtained from analogous reactions using $Rb[BAr^F]$ and $Cs[BAr^F]$, presumably as a result of trace hydrolysis.

Computational details

DFT calculations were performed on the isolated cations $[M(Me_3tacn)]^+$, $[M(Me_3tacn)_2]^+$, and $[M(Me_6[18]aneN_6)]^+$, with M = Li, Na, K, Rb, and Cs, using the BP86 and B3LYP functionals with a 6-311G(d,p) basis set. Further details are given in the ESI.†

Results and discussion

In view of the limited literature examples of aza-macrocyclic complexes with Group 1 cations, their expected lability in solution, and the lack of diagnostic spectroscopic signatures for these complexes, X-ray crystallographic data provide the key characterisation method. We therefore describe the solid state data first, comparing these with computed structures obtained using DFT, followed by their solution NMR spectroscopic data.

DFT calculations were carried out using the BP86 and B3LYP functionals. In general, these functionals perform equally well in replicating bond distances and angles in the cations investigated (Tables S2, S3, S7, S8 and S12–S23†). The results from the BP86 functional are discussed in the main manuscript, while those computed with the B3LYP functional are collected in the ESI.†

Hexa-aza macrocyclic complexes

The reaction of $[Li(thf)_4][BAr^F]$ with $Me_6[18]aneN_6$ in CH_2Cl_2 led to the isolation of a white crystalline solid (Scheme 1) which was formulated as $[Li(Me_6[18]aneN_6)][BAr^F]$ on the basis of microanalytical, ^{1}H, $^{13}C\{^1H\}$, and ^{7}Li NMR spectroscopic data. The crystal structure (Fig. 1) shows the $[Li(Me_6[18]aneN_6)]^+$ cation contains an N_6 donor set (without retention of thf) and the macrocycle is in a puckered conformation; the distortion from an ideal octahedron is severe, as seen by two

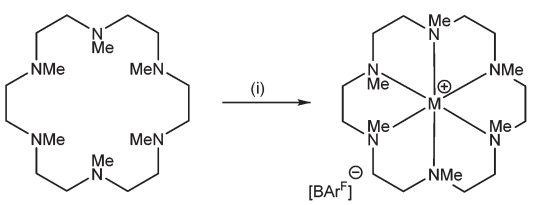

Scheme 1 Synthesis of $Me_6[18]aneN_6$ complexes. Conditions: (i) M = Li: $[Li(thf)_4][BAr^F]$, CH_2Cl_2; M = Na: $Na[BAr^F]\cdot 2thf$, CH_2Cl_2; M = K, Rb, Cs: $M[BAr^F]$, CH_2Cl_2.

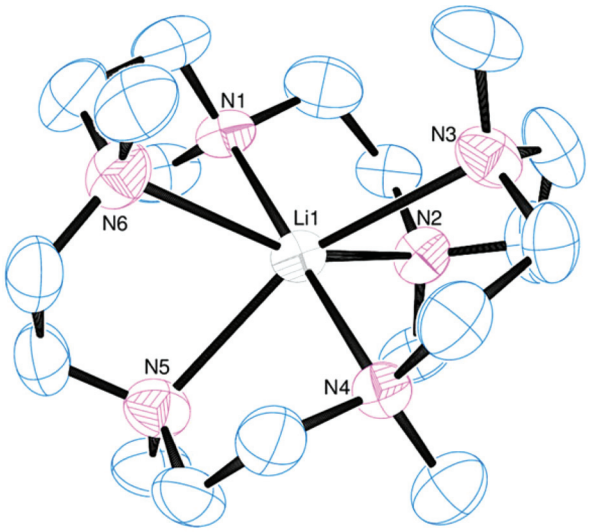

Fig. 1 View of the cation in $[Li(Me_6[18]aneN_6)][BAr^F]$. Thermal ellipsoids are drawn at 50% probability. H atoms and the $[BAr^F]^-$ anion are omitted for clarity. Selected bond lengths (Å) and angles (°): Li–N1 2.274(9), Li–N2 2.384(9), Li–N3 2.587(9), Li–N4 2.315(9), Li–N5 2.45(1), Li–N6 2.554(9); N1–Li–N2 77.3(3), N2–Li–N3 73.1(3), N3–Li–N4 74.3(3), N4–Li–N5 77.7(3), N5–Li–N6 73.5(3), N6–Li–N1 75.9(3).

of the '*trans*' N–Li–N angles which show a large deviation from 180°, whilst the Li–N bond lengths vary by *ca.* 0.3 Å. They are longer than the sum of ionic radii for Li (6-coordinate) and N (2.39 Å),[20] but significantly shorter than the sum of van der Waals radii (3.78 Å),[21] consistent with the mismatch between the small Li^+ cation and the 18-membered ring. The ^{1}H NMR spectrum is broad at 298 K, indicating dynamic behaviour in solution, while the ^{7}Li NMR spectrum shows a singlet at −0.30 ppm.

The computed minimum energy geometry of the isolated $[Li(Me_6[18]aneN_6)]^+$ cation (Fig. 2) has C_2 symmetry. The macrocycle is puckered as in the crystal structure, and overall the computed geometric parameters are also in good agreement with the experimental values (Tables S2 and S3†).

Fig. 3 shows the isodensity plots of the frontier molecular orbitals (FMOs) of $[Li(Me_6[18]aneN_6)]^+$. The results show that the highest occupied molecular orbital (HOMO) is centred on the six N atoms of the $Me_6[18]aneN_6$ ring, and is composed of the N 2p lone pairs with their associated lobes oriented in the direction of the Li^+ ion. Population analysis shows that the low-lying HOMOs (HOMO−1 to HOMO−5) are also dominated by the N 2p lone pairs, however, an increasing contribution of Li^+ is observed from HOMO−1 to HOMO−5 (*i.e.* HOMO−1, HOMO−3, HOMO−4, and HOMO−5 have 3%, 6%, 6%, and 10% contributions from the $2p_z$, $2p_x$, $2p_y$, and 2s orbitals of Li^+, respectively). LUMO and LUMO+1 are antibonding molecular orbitals (ABMOs) and correspond predominantly to the 2s and 2p orbitals of the Li^+ centre.

$[Na(Me_6[18]aneN_6)][BAr^F]$ was also isolated as a white solid from the reaction of $Na[BAr^F]\cdot 2thf$ with $Me_6[18]aneN_6$ and similarly characterised. Whilst we were unable to grow crystals

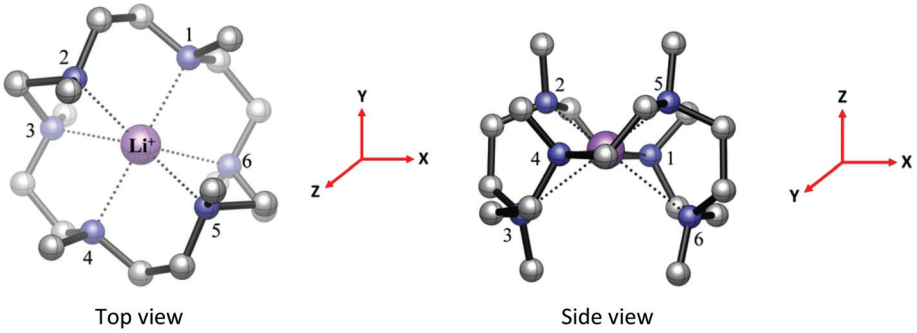

Fig. 2 The optimised BP86 DFT geometry of the $[Li(Me_6[18]aneN_6)]^+$ cation with C_2 symmetry and ^1A electronic ground state. The reference axes are shown (in red).

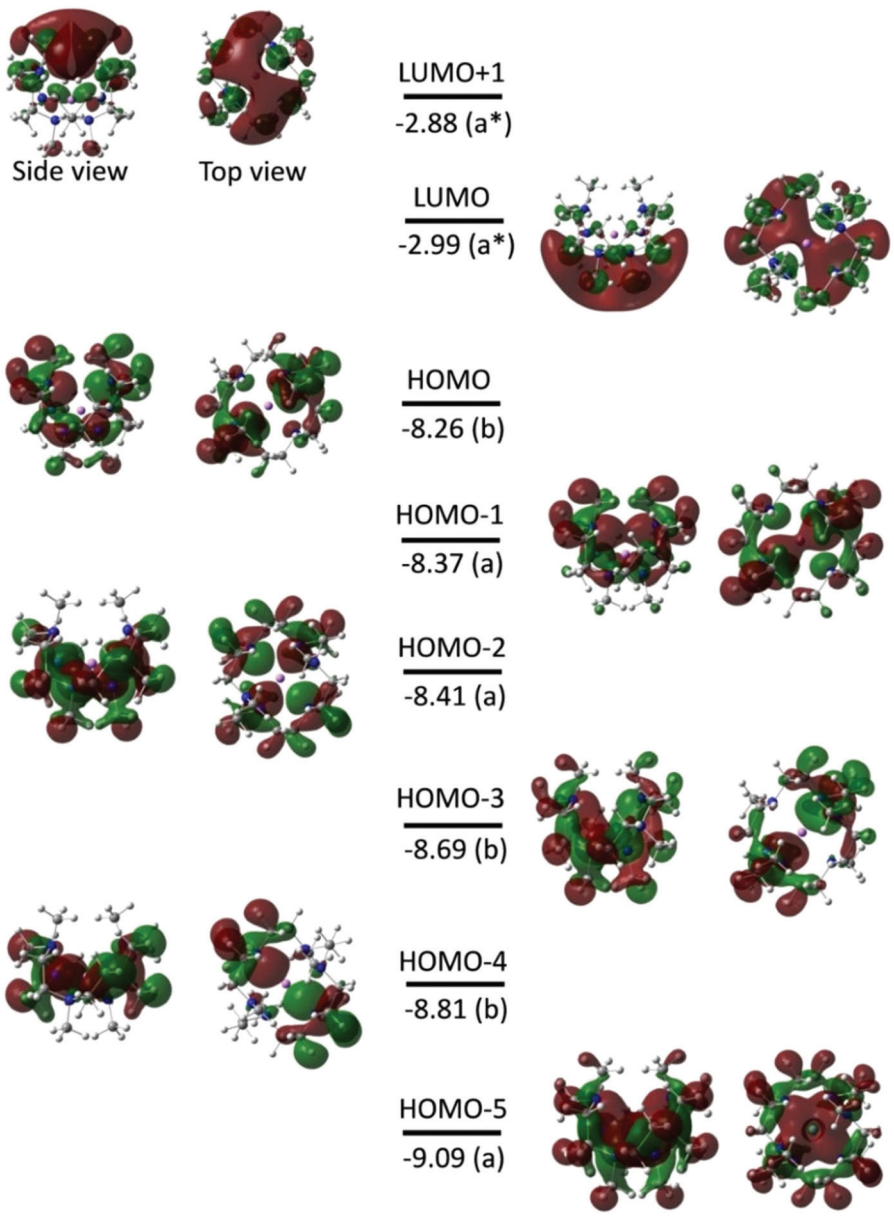

Fig. 3 Frontier molecular orbitals (isovalue of 0.02 electrons $Bohr^{-3}$) for the $[Li(Me_6[18]aneN_6)]^+$ complex obtained from BP86 DFT calculations. The energy and symmetry of the molecular orbitals are given in eV and in parentheses, respectively. The dark red (+) and green (–) lobes represent the signs of the angular part of the AO contributing to a MO.

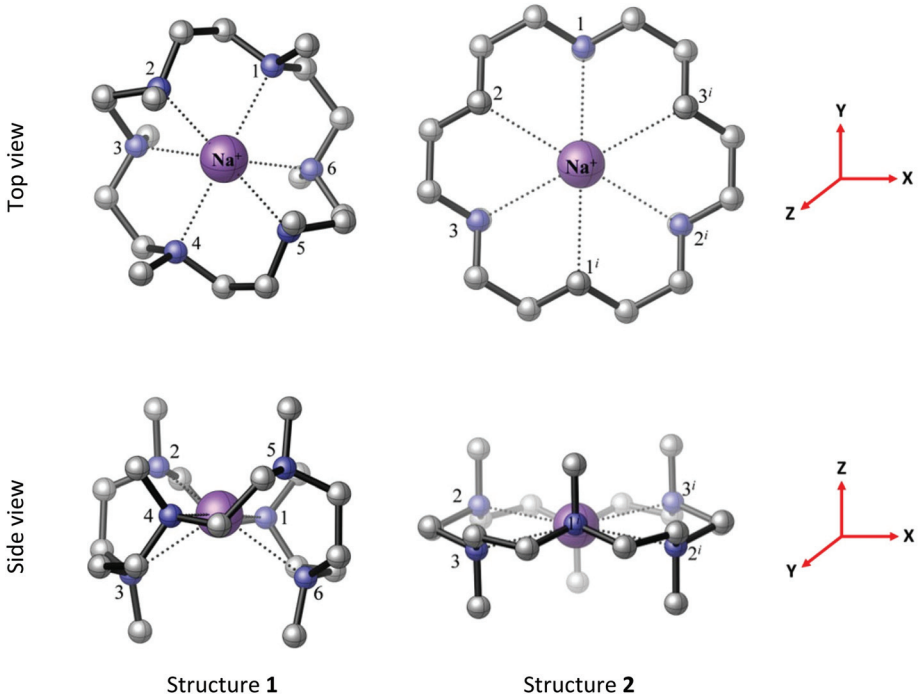

Fig. 4 The BP86 DFT optimised geometries of $[Na(Me_6[18]aneN_6)]^+$ structures **1** (C_2 symmetry) and **2** (D_{3d} symmetry). The reference axes are shown (in red). Structure **1** is computed to be more stable than structure **2** by 28.2 kJ mol^{-1}.

suitable for X-ray analysis, hexadentate coordination of the macrocycle is likely. Two possible minimum energy structures of $[Na(Me_6[18]aneN_6)]^+$ (**1** and **2** in Fig. 4) were located in the BP86 DFT calculations. Structure **1** (C_2 symmetry) is analogous to the computed minimum energy structure of $[Li(Me_6[18]aneN_6)]^+$, while structure **2** (D_{3d} symmetry) has a geometry similar to its K^+ and Rb^+ counterparts (*vide infra*). Structure **1** is more stable than **2** by 28.2 kJ mol^{-1} in the gas phase (Tables S12, S13, S18 and S19†). It is important to note that the presence of the $[BAr^F]^-$ anions in the crystal will influence the relative stabilities of structures **1** and **2** in the isolated solids.

$[K(Me_6[18]aneN_6)][BAr^F]$ was isolated and characterised similarly. Its X-ray structure (Fig. 5) showed two half-cations in the asymmetric unit, with the K^+ ions occupying crystallographic inversion centres. $[K(Me_6[18]aneN_6)]^+$ shows hexagonal planar N_6 coordination at K^+, with the NMe groups alternating 'up-down' around the ring. The difference between the two K^+ cations in the asymmetric unit is found in the long-range interactions to the $[BAr^F]^-$ anions. There are two K2···F1 inter-

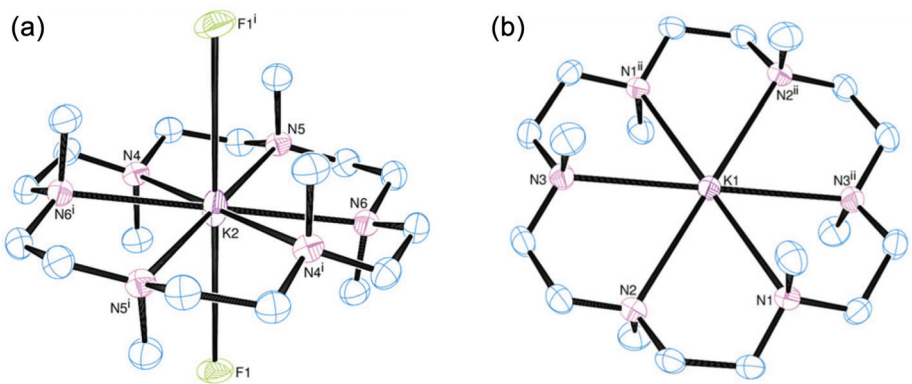

Fig. 5 (a) View of the K2 centred cation (left) and (b) the K1 cation (right) of $[K(Me_6[18]aneN_6)][BAr^F]$. Thermal ellipsoids are drawn at 50% probability. H atoms and the $[BAr^F]^-$ anions (bar F1) are omitted for clarity. Selected bond lengths (Å) and angles (°): K1–N1 2.883(2), K1–N2 2.896(2), K1–N3 2.911(2), K2–N4 2.918(2), K2–N5 2.866(2), K2–N6 2.911(2); N1–K1–N2 61.86(5), N2–K1–N3 61.35(5), N1–K1–N3^{ii} 60.67(5), N4–K2–N5 61.79(5), N5–K2–N6 61.11(5), N4–K1–N6^{i} 61.04(5). Symmetry codes: (i) 1 – *x*, –*y*, 1 – *z*; (ii) –*x*, 1 – *y*, –*z*.

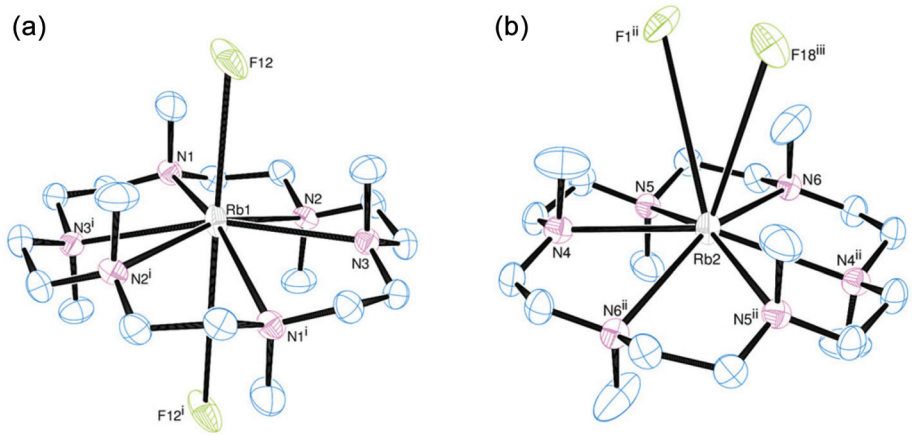

Fig. 6 (a) View of the cation based on Rb1 (left) and (b) view of the cation based on Rb2 (right) of $[Rb(Me_6[18]aneN_6)][BAr^F]$ in the asymmetric unit. Thermal ellipsoids are drawn at 50% probability. H atoms and the $[BAr^F]^-$ anion (bar coordinating fluorines) are omitted for clarity. Selected bond lengths (Å) and angles (°): Rb1–N1 2.899(2), Rb1–N2 2.980(2), Rb1–N3 2.948(2), Rb1···F12 3.235(2), Rb1···F12^i 4.128(1), Rb2–N4 2.921(2), Rb2–N5 2.924(2), Rb2–N6 2.902(2), Rb2···F18^{iii} 3.951(1), Rb2···F1^{ii} 4.233(1); N1–Rb1–N2 61.78(6), N2–Rb1–N3 60.09(6), N1–Rb1–N3^i 60.95(6), N4–Rb2–N5 60.04(6), N5–Rb2–N6 60.50(6), N4–Rb2–N6^{ii} 59.50(6). Symmetry code: (i) $-x$, $2-y$, $-z$; (ii) $1-x$, $1-y$, $1-z$; (iii) $x+1$, y, z.

actions of 3.658(1) Å perpendicular to the N_6 plane (ΣvdW = 4.19 Å),[22] which gives K2 an overall hexagonal bipyramidal arrangement (Fig. 5a). The other potassium cation (K1) contains no K···F interactions and is therefore hexagonal planar (Fig. 5b).

$[Rb(Me_6[18]aneN_6)][BAr^F]$ also crystallises with two Rb^+ cations in the asymmetric unit, with the Rb^+ ion sitting out of the N_6 plane by 0.561(3) Å (Rb1) and 0.382(3) Å (Rb2). For Rb1, this has the effect that one Rb···F interaction is much shorter than the other. The Rb1–F12 distance of 3.235(2) Å is much shorter than the sum of van der Waals radii (4.67 Å) (Fig. 6a),[21] and is also significantly shorter than the corresponding K···F distance. The Rb1···F12^i distance (4.128(1) Å) is also within the sum of van der Waals radii. Rb2 has two long Rb···F distances of 3.951(1) and 4.233(1) Å, both of which are on the same side of the N_6 ring (Fig. 6b).

The BP86 DFT calculations satisfactorily reproduce the experimental X-ray structures of $[M(Me_6[18]aneN_6)]^+$ (M = K and Rb) with D_{3d} symmetry (Fig. 7), which contrasts with C_2 symmetry identified for the Li^+ counterpart. In the computed structures both metal cations lie within the plane of the $Me_6[18]aneN_6$ ring, with six equivalent bond distances (K–N =

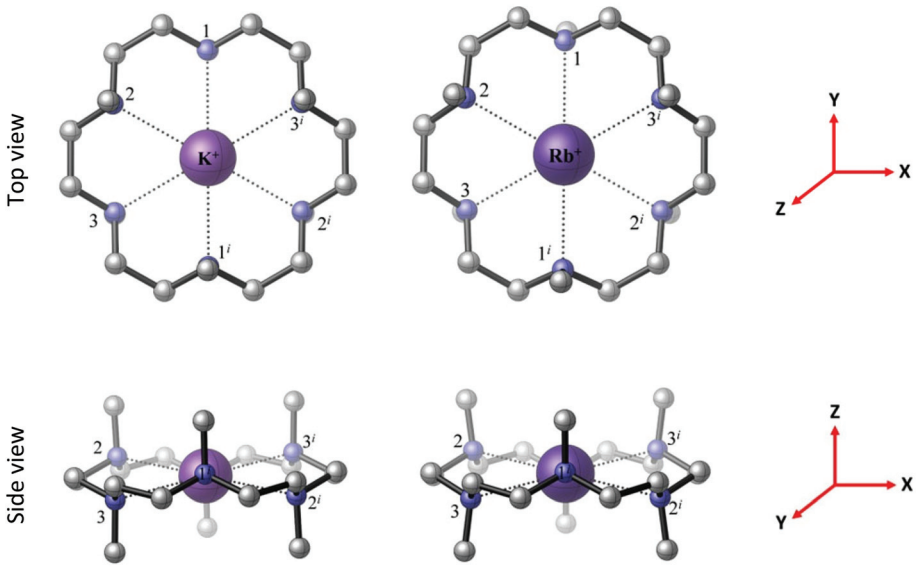

Fig. 7 The BP86 DFT optimised geometries of the $[M(Me_6[18]aneN_6)]^+$ complexes, M = K, Rb, both with D_{3d} symmetry and a $^1A_{1g}$ electronic ground state. The reference axes are shown (in red).

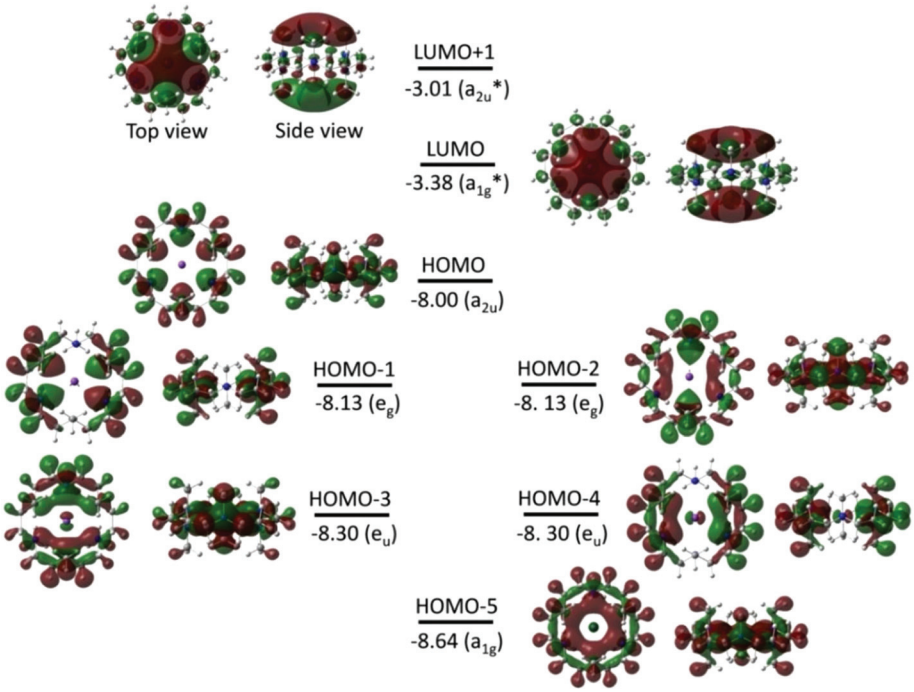

Fig. 8 Frontier molecular orbitals (FMOs) (isovalue of 0.02 electrons Bohr^{-3}) for $[K(Me_6[18]aneN_6)]^+$ obtained from BP86 DFT calculations. The energy and symmetry of the MOs are given in eV and in parentheses, respectively. The dark red (+) and green (–) lobes represent the signs of the angular part of the AO contributing to a MO.

2.984 Å; Rb–N = 3.062 Å), indicating that despite the $[BAr^F]^-$ anion being large and usually considered as very weakly interacting, in some cases it still influences the experimentally determined geometry.

Fig. 8 and S3† show the isodensity plots of the frontier MOs (FMOs) of the $[M(Me_6[18]aneN_6)]^+$ (M = K or Rb, respectively), which are very similar. As for the Li^+ complex discussed above, the HOMO corresponds mainly to the 2p orbitals of N atoms, and the LUMO (and LUMO+1) correspond predominantly to the ns (np) orbitals of K^+ and Rb^+ respectively; the main metal contribution is in the lower HOMO−3 to HOMO−5 orbitals.

The relevant charge densities for the complex cations are shown in Table 1, together with those for $Me_6[18]aneN_6$ itself (which has two conformers of very similar energy, structures **3** and **4**, Fig. S2†). This shows that electron density is transferred from the bonding σ C–H and σ C–N orbitals and N 2p non-bonding orbitals of $[M(Me_6[18]aneN_6)]^+$ to the ns and np valence orbitals of the metal. The metal ion in the $[M(Me_6[18]aneN_6)]^+$ species is more positively charged on going from $Li^+ \rightarrow K^+ \rightarrow Rb^+$, consistent with more electron density being retained on the ligand as Group 1 is descended.

Table 1 Charge densities (natural charge, *e*) on the M (Li, K, Rb) and N centres from BP86 DFT calculations

Centres	M	N
$Me_6[18]aneN_6$ (structure **3**)[a]	—	−0.503 (N3/6), −0.512 (N2/5), −0.515 (N1/4)
$Me_6[18]aneN_6$ (structure **4**)[a]	—	−0.493
$[Li(Me_6[18]aneN_6)]^+$	0.522	−0.529 (N3/6), −0.544(N2/5), −0.548 (N1/4)
$[K(Me_6[18]aneN_6)]^+$	0.734	−0.531
$[Rb(Me_6[18]aneN_6)]^+$	0.934	−0.543

[a] The structures of the optimised geometry of $Me_6[18]aneN_6$, labelled as **3** and **4**, are provided in Fig. S2.

Crystals of $[Cs(Me_6[18]aneN_6)][BAr^F]$ all showed severe disorder, although microanalytical and spectroscopic data were consistent with the formulation $[Cs(Me_6[18]aneN_6)][BAr^F]$. Two possible minimum energy structures for the $[Cs(Me_6[18]aneN_6)]^+$ complex, **5** and **6**, are located by the BP86 DFT computations, with structure **5** lower in energy than structure **6** by 43.1 kJ mol^{-1} (Fig. 9). In **5**, the Cs^+ ion lies out of the N_6 plane by 0.869 Å, similar to the experimentally derived $[Rb(Me_6[18]aneN_6)]^+$ structure. Notably, the reported $[Cs(Me_6[18]aneN_6)]^+$ is structurally very different.[11a]

The bond dissociation energies calculated for $[M(Me_6[18]aneN_6)]^+ \rightarrow M^+ + Me_6[18]aneN_6$ (1) (Table 2) decrease on going from Li^+ to Cs^+, as expected.

Tri-aza macrocyclic complexes

Based upon our earlier work on Na-Me_3tacn complexes,[3] we also attempted to extend the chemistry of Me_3tacn to the other members of Group 1 (Scheme 2).

Using a 1 : 2 molar ratio of $[Li(thf)_4][BAr^F]$: Me_3tacn in toluene resulted in the isolation of the half-sandwich complex $[Li(Me_3tacn)(thf)][BAr^F]$ in good yield. This contrasts with the

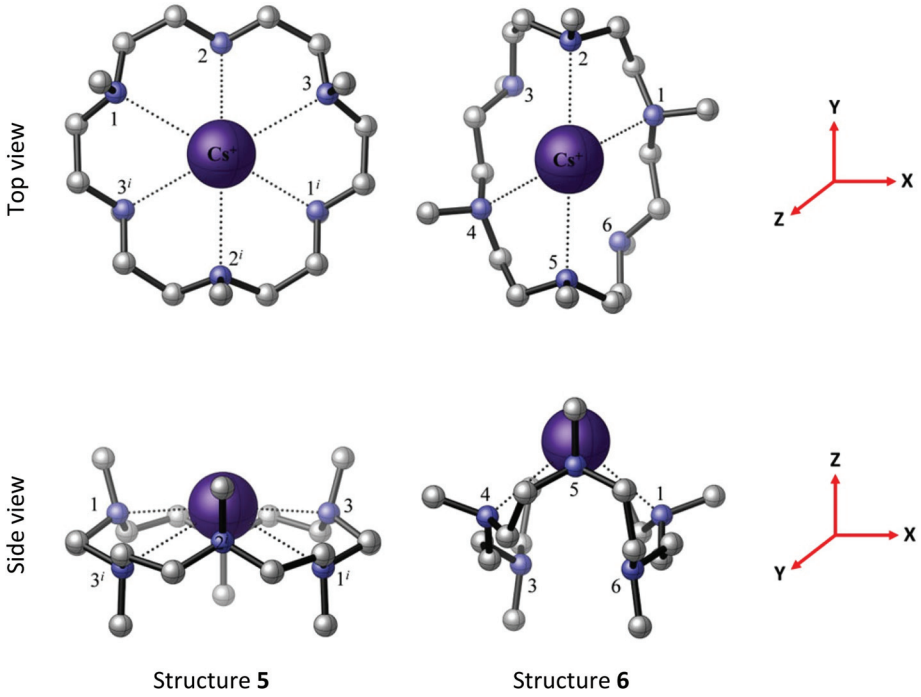

Fig. 9 The BP86 DFT optimised geometries of $[Cs(Me_6[18]aneN_6)]^+$ structures **5** (C_{3v} symmetry) and **6** (C_2 symmetry). The reference axes are shown (in red). Structure **5** is computed to be 43.1 kJ mol^{-1} lower than structure **6**.

Table 2 Zero-point and BSSE corrected BP86 bond dissociation energies[a] (kJ mol^{-1}) for dissociation $[M(Me_6[18]aneN_6)]^+ \rightarrow M^+ + Me_6[18]aneN_6$ (1), M = Li, Na, K, Rb, or Cs

M	(1)
Li	423.3 (421.5)[b]
Na	341.0 (339.2)
K	264.6 (262.9)
Rb	209.1 (207.3)
Cs	151.9 (150.1)

[a] The reported values were obtained using the energy of the $Me_6[18]aneN_6$, structure **4** (Fig. S2). [b] The values in parentheses were obtained using the energy of the $Me_6[18]aneN_6$, structure **3** (Fig. S2).

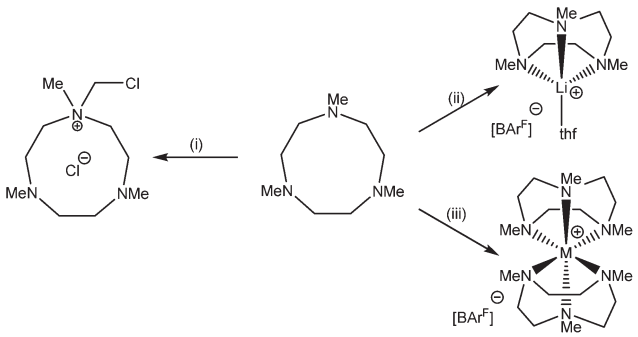

Scheme 2 Products from the reaction of M[BAr^F] with 2 mol. equiv. of Me_3tacn (M = Li, Na, K). Conditions: (i) 0.5 mol. equiv. $[Li(thf)_4][BAr^F]$, CH_2Cl_2; (ii) 0.5 or 1 mol. equiv. $[Li(thf)_4][BAr^F]$, toluene; (iii) M = Na: 0.5 mol. equiv. $Na[BAr^F]\cdot 2thf$, CH_2Cl_2; M = K: 0.5 mol. equiv. $K[BAr^F]$, CH_2Cl_2.

analogous reaction with Na^+, for which both the sandwich and half-sandwich complexes were obtained depending upon the molar ratio of metal : ligand used. Further attempts to form the sandwich $[Li(Me_3tacn)_2]^+$ cation from $[Li(thf)_4][BAr^F]$ and 2 mol. equiv. of Me_3tacn in CH_2Cl_2 instead led to a quaternary ammonium cation as its chloride salt (Scheme 2), which was identified by ^{1}H NMR spectroscopy and from comparison with the literature unit cell.[22] No evidence for the $[Li(Me_3tacn)_2]^+$ cation was observed.

Although attempts to crystallise the $[Li(Me_3tacn)(thf)][BAr^F]$ were unsuccessful, its identity is clear from the spectroscopic and analytical data. DFT calculations on the Me_3tacn complexes with Na^+ and Li^+ were undertaken to probe their relative stabilities. The computed bond distances and angles at Na^+ in $[Na(Me_3tacn)_2]^+$ (Fig. 10, Tables S7 and S8†) agree well with the experimental values reported earlier.[3] For Li^+, the calculations show that the Li–N bond in $[Li(Me_3tacn)_2]^+$ (S_6 symmetry) is very long (2.460 Å), whereas in the half-sandwich cation $[Li(Me_3tacn)]^+$ the Li–N distance of 2.029 Å (Fig. 10) is more akin to the reported Li–N bond distances.[9,23] This strongly suggests that the much smaller Li^+ ion can comfortably accommodate only one Me_3tacn (consistent with the isolation of the $[Li(Me_3tacn)(thf)][BAr^F]$ half-sandwich), but introducing a second Me_3tacn is much less favourable, due to steric clashing between the Me groups on the two rings. As noted earlier,[3] the isolation of the bis-Me_3tacn sandwich cation is unusual; the large ionic radius of Na^+ apparently permitting its formation (the Ag^+ analogue is the only other structurally authenticated example).[24]

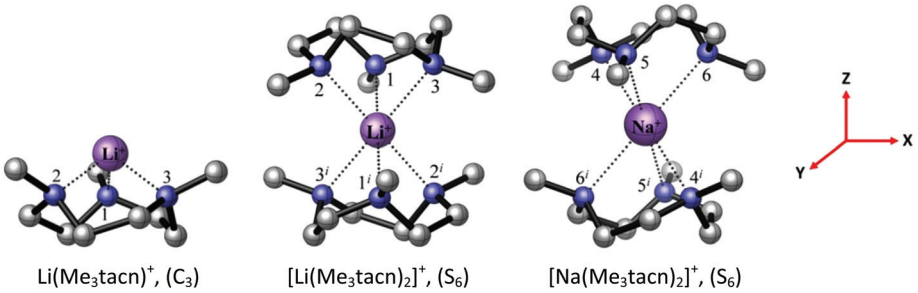

Fig. 10 The BP86 DFT optimised geometry of the $[Li(Me_3tacn)]^+$ and $[M(Me_3tacn)_2]^+$ complexes, M = Li, Na. The symmetry of each complex is given in parentheses. The reference axes are shown (in red).

$[K(Me_3tacn)_2][BAr^F]$ was successfully prepared and isolated similarly to the Na^+ analogue and is isostructural (Fig. 11), forming a centrosymmetric very distorted octahedral cation. This contrasts with the hexagonal planar coordination present in $[K(Me_6[18]aneN_6)]^+$, although the bond distances and angles at K^+ are actually quite similar.

The K–N bonds are 0.2–0.3 Å longer than the corresponding Na–N bonds, while the intra-macrocyclic N–K–N angles are more acute by 8–9°. These differences may reflect a poorer match between the large K^+ cation and the small nine-membered Me_3tacn ring, although as we have noted, they are similar to the angles in $[K(Me_6[18]aneN_6)]^+$. As shown in Fig. 11, the Me groups of the two rings are well separated.

In contrast to the BP86 DFT optimised $[Li(Me_3tacn)_2]^+$ and $[Na(Me_3tacn)_2]^+$ complexes (S_6 symmetry), $[K(Me_3tacn)_2]^+$ is computed to have D_3 symmetry (Fig. 12). The computed K–N bond distances are 2.915 Å; slightly longer than the experimental values (2.765(5)–2.880(5) Å), while the calculated N–K–N bond angles within the five-membered chelate rings (63.0°) are closely comparable to the crystallographic values.

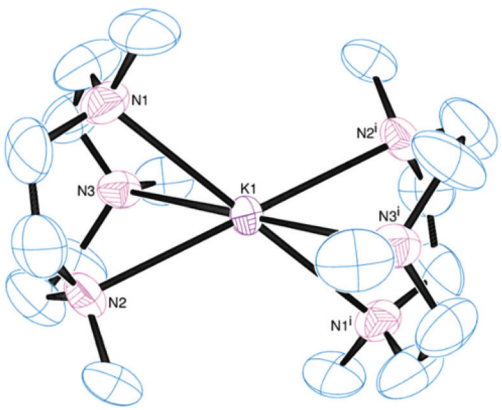

Fig. 11 View of the cation based on K1 in the asymmetric unit of $[K(Me_3tacn)_2][BAr^F]$. Thermal ellipsoids are drawn at 50% probability. H atoms, the $[BAr^F]^-$ anion, and the other half cation are omitted for clarity. Selected range of bond lengths (Å) and angles (°): K1–N1 2.815(6), K1–N2 2.768(5), K1–N3 2.881(6), K2–N4 2.768(6), K2–N5 2.821(6), K2–N6 2.808(6); N1–K1–N2 63.2(2), N2–K1–N3 62.8(2), N3–K1–N1 63.2(2), N4–K2–N5 64.2(2), N5–K2–N6 63.9(2), N6–K2–N4 64.2(2). Symmetry code: (i) 1 – *x*, –*y*, 1 – *z*.

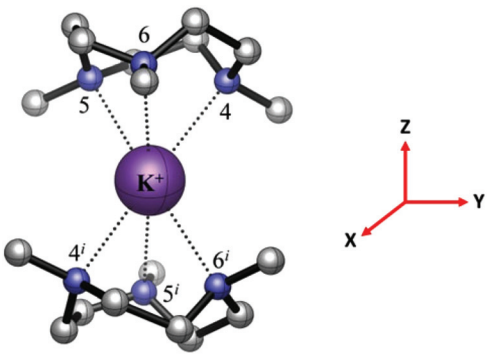

Fig. 12 The BP86 DFT optimised geometry of the $[K(Me_3tacn)_2]^+$ complex with D_3 symmetry and $^1A_1$ electronic ground state. The reference axes are shown (in red).

The calculations on $[K(Me_3tacn)_2]^+$ show that the HOMO and HOMO−1 are doubly degenerate (as are HOMO−2 and HOMO−3) (Fig. 13), and they are mainly located on the N atoms of the Me_3tacn ring, corresponding to N 2p valence orbitals. The LUMO, LUMO+1 and LUMO+2 are mainly localised on K^+. The LUMO corresponds to the 4s orbital of K^+, while LUMO+1 and LUMO+2 correspond mainly to the $4p_x$ and $4p_y$ orbitals, respectively. The FMOs of the $[Na(Me_3tacn)_2]^+$ analogue follow similar trends (Fig. S5†).

Table 3 shows the charge densities on the metal and N atoms of Me_3tacn, $[M(Me_3tacn)]^+$ and $[M(Me_3tacn)_2]^+$, M = Na and K. The natural charge on K^+ is lower than the formal charge of +1, showing a significant electron density transfer from the ligands. The charge densities on the N atoms for $[M(Me_3tacn)]^+$ and $[M(Me_3tacn)_2]^+$ are more negative than in the 'free' ligand, because electron density is withdrawn from σ C–H and σ C–N orbitals of the ligand.

As in the $[M(Me_6[18]aneN_6)]^+$ analogues, the charge densities on M show that less electron density is transferred to the metal in the K^+ case, suggesting a relatively weaker interaction between the K^+ and the Me_3tacn ligand(s), and correspondingly longer K–N distances, than in the Na^+ case.

Attempts to prepare analogous complexes with Rb^+ and Cs^+ ions failed; the optimised minimum energy structures of $[M(Me_3tacn)_2]^+$ (M = Rb, Cs) are presented in Tables S16, S17, S22 and S23.†

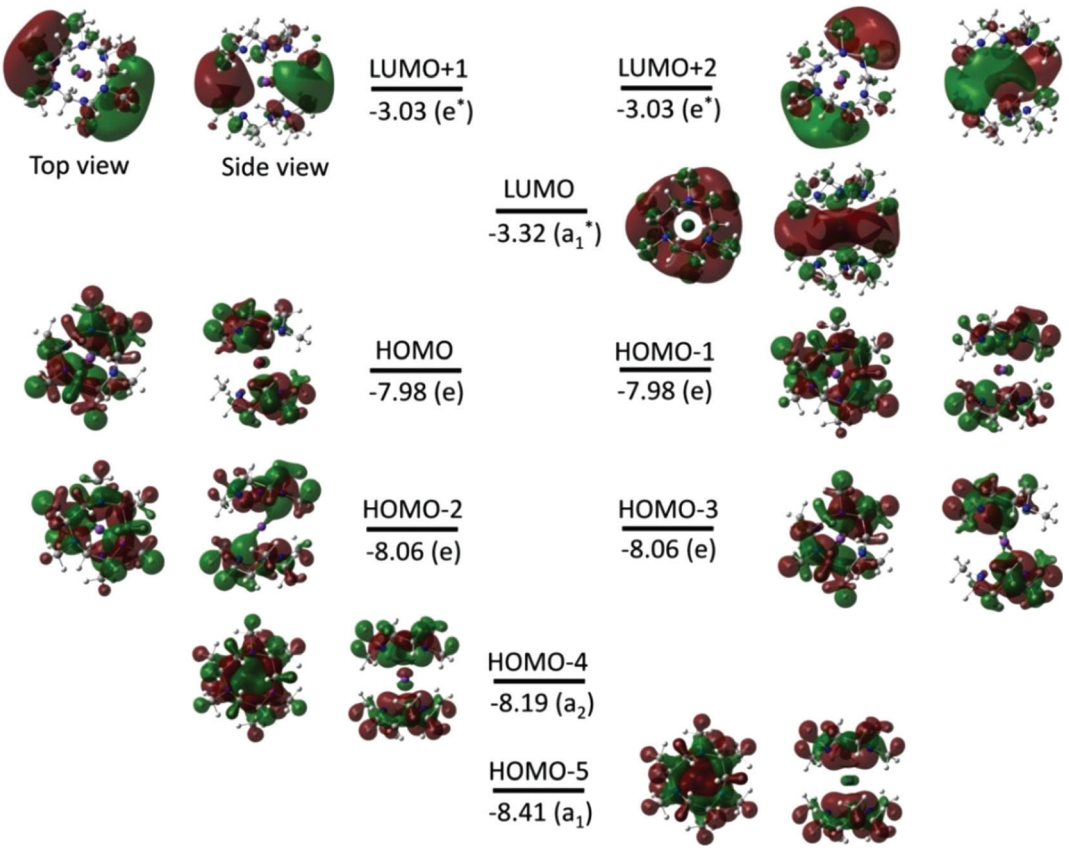

Fig. 13 FMOs (isovalue of 0.02 electrons Bohr^{-3}) for the $[K(Me_3tacn)_2]^+$ complex obtained from BP86 DFT calculations. The energy and symmetry of the MOs are given in eV and in parentheses, respectively. The dark red (+) and green (–) lobes represent the signs of the angular part of the AO contributing to a MO.

Table 3 Charge densities (natural charge, e) on the Na, K, and N centres obtained from BP86 DFT calculations

	M = Na		M = K	
Centres	Na	N	K	N
Me_3tacn	—	−0.499	—	−0.499
$[M(Me_3tacn)]^+$	+0.867	−0.587	+0.913	−0.575
$[M(Me_3tacn)_2]^+$	+0.551	−0.549	+0.680	−0.542

Table 4 Zero-point and BSSE corrected BP86 bond dissociation energies (kJ mol^{-1}) for the dissociation $[M(Me_3tacn)]^+ \rightarrow M^+ + Me_3tacn$ (2) and $[M(Me_3tacn)_2]^+ \rightarrow [M(Me_3tacn)]^+ + Me_3tacn$ (3), M = Li, Na, K, Rb, and Cs

M	(2)	(3)
Li	350.4	63.9
Na	234.0	104.5
K	165.5	86.5
Rb	122.0	77.4
Cs	96.2	63.2

Zero-point and BSSE corrected bond dissociation energies (kJ mol^{-1}) for the dissociation $[M(Me_3tacn)]^+ \rightarrow M^+ + Me_3tacn$ (2), M = Li, Na, K, Rb, and Cs, decrease on going down Group 1 (Table 4), correlating with the increase in the ionic radii, and the poorer fit with the small triaza macrocycle. A similar trend in zero-point corrected bond dissociation energies is observed for the dissociation of $[M(Me_3tacn)_2]^+ \rightarrow [M(Me_3tacn)]^+ + Me_3tacn$ (3), except for the dissociation energy of the $[Li(Me_3tacn)_2]^+$ complex which is much lower. This appears to be mainly a consequence of the inability of the small lithium ion to accommodate six-coordination because the presence of the Me substituents on one macrocycle sterically impedes the approach of the second.

It seems clear, therefore, that isolation of the $[M(Me_3tacn)_2]^+$ cations is a fine balance between the metal ion being sufficiently large to avoid significant steric clashing between the Me groups of the two rings, but small enough to avoid very acute N–M–N chelate angles.

Tetra-aza macrocyclic complexes

Changing the ligand from Me_3tacn to $Me_4cyclen$ has the effect of both increasing the denticity and expanding the macrocyclic binding cavity. Reaction of $[Li(OH_2)_4][BAr^F]$ with $Me_4cyclen$ in

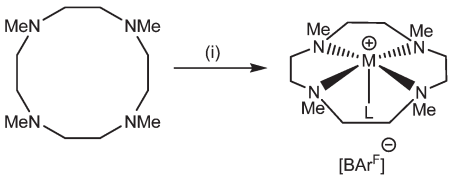

Scheme 3 Reaction of M[BAr^F] with Me_4cyclen. Conditions: (i) M = Li: $[Li(OH_2)_4][BAr^F]$, CH_2Cl_2, L = H_2O; M = Na: Na[BAr^F]·2thf, CH_2Cl_2, L = thf.

CH_2Cl_2 (Scheme 3) led to the formation of $[Li(Me_4cyclen)(OH_2)][BAr^F]$.

The crystal structure shows a five-coordinate square pyramidal (τ = 0.02)[25] cation with the macrocycle tetradentate and one apical water molecule (Fig. 14). The NMe groups all lie on the same side of the N_4 plane as the metal, with the Li cation displaced out of the N_4 plane by 0.758(7) Å. The same product is obtained irrespective of the ratio of Me_4cyclen : Li[BAr^F] used.

The reaction between Me_4cyclen and Na[BAr^F]·2thf in CH_2Cl_2 yielded $[Na(Me_4cyclen)(thf)][BAr^F]$, with the thf ligand apical (Fig. 15). The τ value of 0.00 confirms an ideal square-based pyramidal geometry and the sodium cation is out of the N_4 plane by 1.225(2) Å.

Although sandwich complexes of the Group 1 cations with 12-crown-4, *e.g.* $[Na(12\text{-crown-}4)_2]^+$, are well known,[1] over the course of our studies we found no evidence for $[M(Me_4cyclen)_2]^+$ sandwich cations. Attempts to synthesise the half-sandwich $[M(Me_4cyclen)]^+$ salts with the heavier Group 1 cations (K^+, Rb^+, Cs^+) resulted only in the isolation of $[Me_4cyclenH][BAr^F]$.

Solution multinuclear NMR spectroscopy

The ^1H and $^{13}C\{^1H\}$ NMR spectra (Experimental) each show the presence of the coordinated aza-macrocycle. The ^1H NMR spectra of $Me_6[18]aneN_6$ complexes of K^+, Rb^+, and Cs^+ salts at ambient temperatures show broad CH_3 and CH_2 resonances with no resolved coupling evident, indicative of exchanging species. On cooling the solutions the resonances broaden and then split, the effects being most evident in the Cs^+ salt, but even at 185 K the resonances are still broad and lack resolved couplings, showing that the low temperature limiting spectra have not been reached. These effects are reversible with temperature. Upon cooling the $[Cs(Me_6[18]aneN_6)][BAr^F]$ solution, the broad signal for the CH_2 protons resolved into complex multiplets and the resonance for the methyl protons split into sharp singlets. This behaviour is most likely a result of two major stereoisomers (arising from the different orientations of the Me groups: 'all-up' and alternating 'up-down') for which the separate resonances are evident at low temperature as their rate of interconversion slows.

The Group 1 elements offer several nuclei,‡ suitable for NMR spectroscopic studies.[26] Lithium-7 NMR spectra on the aza complexes each show singlet resonances close to δ = 0 (see Experimental). Like the Na^+-aza macrocyclic cations in our earlier work,[3] the ^{23}Na NMR spectra of the new complexes are sharp resonances with chemical shifts to high frequency of Na^+ in water (δ = 0): $[Na(Me_6[18]aneN_6)][BAr^F]$ +3.1; $[Na(Me_4cyclen)(thf)][BAr^F]$ +12.7; $[Na(Me_4cyclam)(thf)][BAr^F]$ +11.4; $[Na(Me_3tacn)(thf)][BAr^F]$ +3.7; $[Na(Me_3tacn)_2][BAr^F]$ +6.2. Although

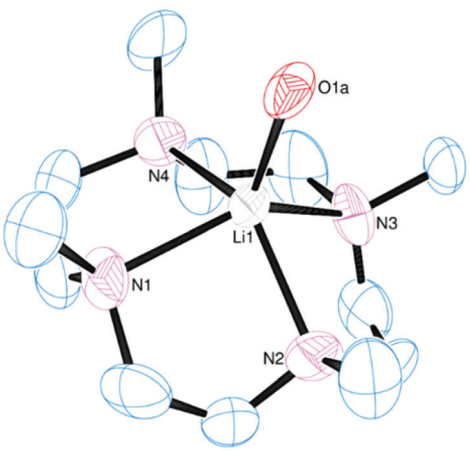

Fig. 14 View of the cation in $[Li(Me_4cyclen)(OH_2)][BAr^F]$. Thermal ellipsoids are drawn at 50% probability. H atoms and the $[BAr^F]^-$ anion are omitted for clarity. Selected bond lengths (Å) and angles (°): Li1–N1 2.186(8), Li1–N2 2.206(8), Li1–N3 2.179(8), Li1–N4 2.154(9), Li1–O1a 1.98(1); N1–Li1–N2 82.8(3), N2–Li1–N3 82.1(3), N3–Li1–N4 84.7(3), N1–Li1–N4 = 82.6(3).

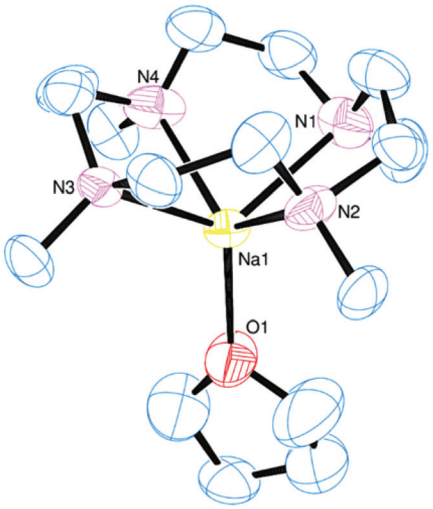

Fig. 15 View of the cation present in $[Na(Me_4cyclen)(thf)][BAr^F]$. Thermal ellipsoids are drawn at 50% probability. H atoms, the $[BAr^F]^-$ anion, and disorder of the ethylene linkers within the Me_4cyclen ring are omitted for clarity. Selected bond lengths (Å) and angles (°): Na–N1 2.463(4), Na–N2 2.461(3), Na–N3 2.453(4), Na–N4 2.444(4), Na–O1 2.244(3); N1–Na–N2 75.4(1), N2–Na–N3 75.6(1), N3–Na–N4 76.0(1), N1–Na–N4 75.5(2).

‡NMR properties:- ^7Li: I = $^3/_2$, N = 92.6%, $R_c = 1.54 \times 10^3$, $Q = -3.7 \times 10^{-30}$ m^2, Ξ = 38.87 MHz; ^{23}Na: I = $^3/_2$, N = 100%, $R_c = 5.24 \times 10^2$, $Q = 0.10 \times 10^{-28}$, Ξ = 26.43; ^{39}K: I = $^3/_2$, N = 93.3%, R_c = 2.69, $Q = 5.5 \times 10^{-30}$, Ξ = 4.67; ^{85}Rb: I = $^5/_2$, N = 72.1%, R_c = 43.4, $Q = 0.25 \times 10^{-28}$, Ξ = 9.69; ^{133}Cs: I = $^7/_2$, N = 100%, $R_c = 2.75 \times 10^2$, $Q = -0.3 \times 10^{-30}$, Ξ = 13.21.

the cations are expected to be exchanging rapidly in solution, these values can be compared with the Na^+-crown ether cations which have chemical shifts to low frequency of 0 ppm, and therefore indicate that the aza macrocycle coordination is retained in CH_2Cl_2 solution.

Solutions of the potassium complexes in CH_2Cl_2 solution do not show a ^{39}K resonance at room temperature (295 K) or on cooling to 185 K. Studies of K^+-crown ether cations over a range of temperatures and K : crown ether ratios in a range of donor solvents show that often only the 'free' K^+ resonance is seen. The $[K(crown)]^+$ is often not observed most likely due to fast quadrupolar relaxation in the low symmetry environment.[26c,d] In $[K(Me_6[18]aneN_6)]^+$ and $[K(Me_3tacn)_2]^+$ it is probable that fast ligand exchange in solution produces low symmetry environments and fast quadrupolar relaxation (the corresponding ^1H NMR spectra show only broad singlets for the macrocyclic CH_2 groups). For similar reasons,[26e] no ^{85}Rb resonance was observed at any temperature between 298 and 185 K.

The Q value for the ^{133}Cs nucleus is small, hence NMR spectra are readily observed. The VT ^{133}Cs NMR data for $[Cs(Me_6[18]aneN_6)][BAr^F]$ show a singlet at 54.1 ppm (298 K) and this splits into two singlets at 73.3 and 58.7 ppm at 183 K, which we attribute to the slowing of dynamic processes and the presence of two significant stereoisomers ('all up' and alternating 'up–down'). These chemical shifts are also significantly to high frequency of those typically observed in crown ether adducts.[26f]

Conclusions

By taking advantage of the lower lattice energies associated with $M[BAr^F]$ precursors, which leads to increased solubility in very weak donor solvents such as CH_2Cl_2, the unusual Group 1 cation complexes $[M(Me_6[18]aneN_6)][BAr^F]$ can be obtained in good yield for all members from M = Li to Cs. Structural characterisation of several of these (M = Li, K, and Rb) allows comparisons down the Group, as well as with the rarely observed bis-Me_3tacn sandwich cations, $[M(Me_3tacn)_2][BAr^F]$, isolated for M = Na and K. The combined experimental and DFT study indicates that the isolation of the $[M(Me_3tacn)_2]^+$ cations requires a fine balance of, on one hand, the metal ion being sufficiently large to avoid significant steric clashing between the Me groups of the two rings, and on the other, the ion being sufficiently small to avoid extremely acute N–M–N chelate angles. In contrast, the very small Li^+ ion forms only the half-sandwich $[Li(Me_3tacn)(thf)]^+$ cation. These complex cations show significant structural differences which correlate closely with the trends in ionic radii down Group 1 and the available macrocyclic binding cavity. The $[BAr^F]^-$ anions also show quite significant M···F interactions, particularly towards the larger metal ions (K^+ and beyond), despite being large, diffuse ions with delocalised charge.

DFT calculations show very good agreement with the experimentally determined structures and confirm significant donation of electron density from the N atoms of the ligand upon complexation, which is accompanied by transfer of some electron density to N from the σ C–H and σ C–N bonding orbitals. The nature of the FMOs show that contributions from the metal orbitals are only significant in the lower energy valence occupied orbitals, while the HOMO itself is dominated by the N 2p orbitals. The calculations also show that coordination of the aza macrocycle to the Group 1 cation in these complexes involves significant donation of electron density from the p-orbitals on the N atoms, rather than purely electrostatic interactions.

Acknowledgements

We thank the EPSRC for supporting the SCFED project through a Programme Grant (EP/I033394/1). The SCFED Project (http://www.scfed.net) is a multidisciplinary collaboration of British universities investigating the fundamental and applied aspects of supercritical fluids. The authors also acknowledge the use of the EPSRC UK National Service for Computational Chemistry Software (NSCCS). This work was also supported by funding provided by the Mauritius Tertiary Education Commission (TEC).

Notes and references

1 J. W. Steed and J. L. Atwood, *Supramolecular Chemistry*, Wiley, 2nd edn, 2009, p. 116.
2 (*a*) T. Hashimoto and K. Maruoka, *Asymmetric Phase Transfer Catalysis*, ed. K. Maruoka, Wiley, Weinheim, 2008, p. 1; (*b*) S. Chun, S. V. Dzyuba and R. A. Bartsch, *Anal. Chem.*, 2001, **73**, 3737; (*c*) J. K. Choi, S. H. Kim, J. Yoon, K.-H. Lee, R. A. Bartsch and J. S. Kim, *J. Org. Chem.*, 2006, **71**, 8011; (*d*) G. W. Gokel, W. M. Leevy and M. E. Weber, *Chem. Rev.*, 2004, **104**, 2723; (*e*) B. P. Hay and R. D. Hancock, *Coord. Chem. Rev.*, 2001, **212**, 61; (*f*) J. W. Steed, *Coord. Chem. Rev.*, 2001, **215**, 171.
3 M. Everett, A. Jolleys, W. Levason, D. Pugh and G. Reid, *Chem. Commun.*, 2014, **50**, 5843.
4 P. Bartlett, D. A. Cook, M. W. George, A. L. Hector, J. Ke, W. Levason, G. Reid, D. Smith and W. Zhang, *Phys. Chem. Chem. Phys.*, 2014, **16**, 9202.
5 J. Clayden, *Organolithiums: Selectivity for Synthesis*, Elsevier Science Ltd., Oxford, 2002.
6 W. Clegg, B. Conway, A. R. Kennedy, J. Klett, R. E. Mulvey and L. Russo, *Eur. J. Inorg. Chem.*, 2011, 721.
7 (*a*) G. W. Gokel, *Chem. Soc. Rev.*, 1992, **21**, 39; (*b*) R. S. Dhillon, S. E. Madbak, F. G. Ciccone, M. A. Buntine, S. F. Lincoln and K. P. Wainwright, *J. Am. Chem. Soc.*, 1997, **119**, 6126; (*c*) H. Tsukube, *J. Chem. Soc., Perkin Trans. 1*, 1989, 1537.
8 (*a*) J. L. Dye, *Prog. Inorg. Chem.*, 1984, **32**, 327; (*b*) J. Kim, M. Shamsipur, S. Z. Huang, R. H. Huang and J. L. Dye, *J. Phys. Chem. A*, 1999, **103**, 5615.

9 (*a*) R. H. Huang, D. L. Ward and J. L. Dye, *Acta Crystallogr., Sect. C: Cryst. Struct. Commun.*, 1990, **46**, 1835; (*b*) J. L. Dye and R. H. Huang, *Pure Appl. Chem.*, 1993, **65**, 435; (*c*) J. Arnold, V. Knapp, J. A. R. Schmidt and A. Shafir, *J. Chem. Soc., Dalton Trans.*, 2002, 3273; (*d*) K. J. Kolonko, I. A. Guzei and H. J. Reich, *J. Org. Chem.*, 2010, **75**, 6163.

10 (*a*) H.-H. Giese, T. Habereder, H. Nöth, W. Ponikwar, S. Thomas and M. Warchhold, *Inorg. Chem.*, 1999, **38**, 4188; (*b*) S. Standfuss, T. P. Spaniol and J. Okuda, *Eur. J. Inorg. Chem.*, 2010, 2987.

11 (*a*) M. E. Kuchenmeister and J. L. Dye, *J. Am. Chem. Soc.*, 1989, **111**, 935; (*b*) A. S. Ellaboudy, C. J. Bender, J. Kim, D.-H. Shin, M. E. Kuchenmeister, G. T. Babcock and J. L. Dye, *J. Am. Chem. Soc.*, 1991, **113**, 2347; (*c*) J. Kim, J. L. Eglin, A. S. Ellaboudy, L. E. H. McMills and S. Huang, *J. Phys. Chem.*, 1996, **100**, 2885.

12 M. Brookhart, B. Grant and A. F. Volpe Jr., *Organometallics*, 1992, **11**, 3920.

13 I. Mon, D. A. Jose and A. Vidal-Ferran, *Chem. – Eur. J.*, 2013, **19**, 2720.

14 K. Wieghardt, P. Chaudhuri, B. Nuber and J. Weiss, *Inorg. Chem.*, 1982, **21**, 3086.

15 S. H. Pine and B. L. Sanchez, *J. Org. Chem.*, 1971, **36**, 829.

16 (*a*) *CrystalClear-SM Expert 3.1 b27*, Rigaku Corporation, Tokyo, Japan, 2012; (*b*) *CrystalClear-SM Expert 2.1 b29*, Rigaku Corporation, Tokyo, Japan, 2013.

17 L. J. Farrugia, *J. Appl. Crystallogr.*, 2012, **45**, 849.

18 A. B. Chaplin and A. S. Weller, *Eur. J. Inorg. Chem.*, 2010, 5124.

19 F. H. Allen, O. Johnson, G. P. Shields, B. R. Smith and M. Towler, *J. Appl. Crystallogr.*, 2004, **37**, 335.

20 R. D. Shannon, *Acta Crystallogr., Sect. A: Cryst. Phys., Diffr., Theor. Gen. Cryst.*, 1976, **32**, 751.

21 S. Alvarez, *Dalton Trans.*, 2013, **42**, 8617.

22 R. D. Ernst, B. G. Harvey, O. J. Oteri and A. M. Arif, *Z. Kristallogr. - New Cryst. Struct.*, 2005, **220**, 373.

23 (*a*) S. Standfuss, T. P. Spaniol and J. Okuda, *Eur. J. Inorg. Chem.*, 2010, 2987; (*b*) Y. Habata, C. Okazaki, K. Ogura, S. Akabori, X. X. Zhang and J. S. Bradshaw, *Inorg. Chem.*, 2007, **46**, 8264.

24 C. Stockheim, K. Wieghardt, B. Nuber, J. Weiss, U. Flörke and H.-J. Haupt, *J. Chem. Soc., Dalton Trans.*, 1991, 1487.

25 A. W. Addison, T. N. Rao, J. Reedijk, J. van Rijn and G. C. Verschoor, *J. Chem. Soc., Dalton Trans.*, 1984, 1349.

26 (*a*) *Multinuclear NMR*, ed. J. Mason, Plenum Press, NY, 1987; (*b*) *NMR and the Periodic Table*, ed. R. K. Harris and B. E. Mann, Academic Press, NY, 1978; (*c*) M. Shporer and Z. Luz, *J. Am. Chem. Soc.*, 1975, **97**, 665; (*d*) J.-S. Shih and A. I. Popov, *Inorg. Chem.*, 1979, **19**, 1689; (*e*) S. Khazaeli, J. L. Dye and A. I. Popov, *Spectrochim. Acta, Part A*, 1983, **39**, 19; (*f*) A. Vendilo, K. Popov, M. Lajunen, V. Chistov, D. Djigailo, H. Rönkkömäki, V. Privalov and I. Pletnev, *Polyhedron*, 2014, **81**, 341.